中國機械工程學刊第四十卷第四期第 327~339 頁(民國一百零八年)
Journal of the Chinese Society of Mechanical Engineers, Vol.40, No.4, pp 327~339 (2019)

Vibration Reduction of Damping Rings on 3D Nonlinear Multi-loaded Slender Beams

Yi-Ren Wang* and Wan-Chi Hsiao**

Keywords：Nonlinear beam, Internal resonance, Vibration reduction, Aeroelasticity.

ABSTRACT

This study examines the damping effects of two damping rings (DRs) applied on an offshore wind-turbine tower (a slender beam) subject to multiple external forces. The wind-turbine tower is simulated by a 3D nonlinear fixed-free elastic beam with a concentrated load applied on the beam tip. The multiple external forces include windward drag force, transverse induced force, the current force under the ocean surface, and the concentrated time-dependent load applied by the turbine on the free end of the tower. The Mindlin-Goodman method is applied to obtain the mode shape function of this beam. The method of multiple scales (MOMS) is employed to analyze the nonlinear problem. An 1:1 internal resonance was observed in this 3D elastic beam. The results indicate that in addition to placing one of the DRs at the maximum amplitude of the beam mode shape, adding the other set of DRs at the ocean currents and aerodynamic forces joint will produce better damping effects.

INTRODUCTION

Among the top 20 wind farm locations in the world selected by 4C Offshore (4C Offshore News 2017), 16 are situated in the Taiwan Strait, which indicates that offshore wind power generation has great potentials for Taiwan. However, offshore wind power generation exerts a severe impact on the ecological environment and living creatures in the neighboring waters, which is caused by the noise of the wind turbines and the vibrations of the wind-turbine towers. Tower vibrations affect the structure of the towers themselves, and the noise that they produce adds to the negative influence on the nearby ecological environment. Finding a way to eliminate vibrations in wind-turbine towers thus became the motivation behind this study.

Vibration reduction in wind-turbine towers has been studied for years; Enevoldsen and Mørk (1996) examined the influence of applying a tuned mass damper (TMD) to the top of a tower and performed optimization analysis using the first structural mode. Colwell and Basu (2009) proposed the use of tuned liquid column dampers (TLCDs) to control the structural vibrations within wind-turbine towers. A TCLD is a U-shaped liquid damper that can effectively make use of the gravitational restoring force produced by displaced liquid to achieve vibration reduction. Moreover, the vibration frequency of the liquid within the TLCD can be used to adjust the natural frequency of the structure, which has been demonstrated to be an effective approach to prevent vibration. Brodersen and Høgsberg (2014) developed a stroke amplifying brace damper that can be installed at the base of a wind-turbine tower; they discovered that with suitable braces, the damper can increase the critical damping ratio of the two lowest modes by 1%. Zhang et al. (2014) provided a controllable active torque actuator model for wind-turbine tower vibrations and demonstrated that the proposed module can effectively mitigate the vibrations in wind turbines during operation.

A comprehensive review of the studies above revealed that all of them regarded wind-turbine towers as linear structures. However, nonlinearity might be considered in elastic beams under the influence of extreme wind forces. In most nonlinear beam problems, the internal resonance (I.R.) is a major point of discussion. Due to nonlinearity, I.R. generally occurs in modes that are not being directly excited by external forces, and for this reason, it is often overlooked. What is interesting is that in common 3-D beams with symmetrical cross-sections, 1:1 I.R. is the most likely to take place among the various degrees of freedom. As its resonant frequency is the same with each other, it is also called prime resonance. For instance, Pai (1990) analyzed the 1:1 prime resonance in a 3D nonlinear composite rotating beam. Nayfeh and Pai (2004) established the linear and nonlinear equations of motion for beams, which encompass 2-D and 3-D; they also provided a

Paper Received July, 2018. Revised October, 2018, Accepted October, 2018, Author for Correspondence: Yi-Ren Wang.

* *Professor, Department of Aerospace Engineering, Tamkang University, NewTaipei City, Tamsui Dist., Taiwan 25137, ROC.*

** *Senior Engineer, Auras Technology Co., Ltd., NewTaipei City, Hsin Chuang Dist., Taiwan 24891, ROC.*

reference platform for future research on I.R. Oguamanam (2003) considered a beam equipped with a mass on the free end. The overall structural center of the mass is not situated at the point of contact between the mass and the beam. Assuming that the beam is subjected to warping and twisting stresses, Oguamanam discovered that the torque of the mass load with regard to the beam contact point has a certain degree of importance to the system natural frequency. Stoykov and Ribeiro (2011) examined the stability of a 3D nonlinear rotating beam based on Timoshenko's theory and took into account the deformation caused by twists and warps. They used Floquet's theory to analyze the stability of the system and determined that 1:1 prime resonance produces supercritical symmetry-breaking bifurcation in beams with a square cross-section. Recently, Wang and Lu (2017) proved that particular elastic foundations or suspension systems can cause 1:3 internal resonance in a beam. Wang et al. (2018) gave analytical solutions for a nonlinear tuned mass damper (TMD) and showed better damping effects on beam vibrations.

With regard to the damping effects of TMD or dynamic vibration absorber (DVA) location on a vibrating body, Wang and Lin (2013) examined a DVA system with two degrees of freedom, developed an internal resonance contour plot (IRCP) and a flutter speed contour plot (FSCP) to prevent I.R., and identified the optimal DVA location for vibration reduction. Wang and Wu (2016) examined vibrations in a nonlinear 3D-string fixed at both ends and rested on a nonlinear elastic foundation. A better damping effect was determined for an optimal range of TMD mass ratio and spring constant. Wang and Kuo (2016) examined the vibrations in a nonlinear beam resting on a nonlinear elastic foundation. They discovered that with a certain spring constant in the elastic foundation, 1:3 I.R. occurs in the 1st and 2nd modes of the system. They prevented I.R. and reduced vibrations by hanging a TMD from the beam. They also considered the damping effects of placing the TMD at the free end of the beam (time-dependent boundary conditions) and at other locations. Their results revealed the best damping effects when the TMD was placed between 0.25l and 0.5l from the fixed end of the beam. Wang and Liang (2015) observed the damping effects of a lumped-mass vibration absorber (LMVA) on a hinged-hinged nonlinear beam resting on a nonlinear elastic foundation. Using a 3D maximum amplitude contour plot (3D MACP), they identified the optimal LMVA parameter combination for vibration reduction. These studies demonstrate that changing the location, mass, spring constant, and damping coefficient of the TMD or DVA is a feasible approach to prevent I.R. and mitigate vibrations.

This study considers a 3D nonlinear beam vertically inserted in a seabed. The bottom end is considered as a fixed support, whereas the top is a free end subject to the forces of the wind turbine. We also assumed that the bottom fourth of the beam is subject to the influence of ocean currents and that the rest of the beam is subject to the influence of wind. The wind turbine blades apply a force of F_T to the top of the tower. The multiple forces applied to the wind-turbine tower are as shown in Fig. 1 (a). Note that this study merely focuses on tower vibrations; the general aerodynamic analysis of the wind-turbine blades was not included. We assumed that the flow of the ocean current only generates windward force F_S. In contrast, the wind above the water surface is sufficient to produce a windward external force and transverse induced aerodynamic force (F_D and F_A). The windward and transverse aerodynamic forces (F_D and F_A) of the tower were assumed to be unsteady forces to examine the vibrations of fluid-structure interactions. Furthermore, we added two damping rings (DRs) to the tower. As shown in Fig. 1 (b), d_1 and d_2 indicate the distances between the DRs and the top of the tower. The present work is focusing on the damping effects of DRs on the internal resonance modes. The damping effects of various DRs locations and various DRs mass and spring constant combinations were examined to obtain the optimal damping effects.

MATHEMATICAL MODEL OF WIND-TURBINE TOWER WITH MULTIPLE EXTERNAL FORCES

Equations of Motion

This study simulated the vibrations in a wind-turbine tower using a straight 3D fixed-free nonlinear beam inserted in a seabed, as displayed in Fig. 1 (a), (b). The coordinate definitions of the wind-turbine tower and the relationships between the DRs and the various external forces are presented in Fig. 1 (b). We overlooked gravity effects and did not consider beam rotation. Based on Newton's 2nd law, Euler's angle transformation, and Taylor series expansion, the equations of motion of the nonlinear beam can be expressed as follows (Nayfeh and Pai, 2004):

$$m\ddot{v} + \bar{c}_y\dot{v} = G'_y \tag{1}$$

$$m\ddot{w} + \bar{c}_z\dot{w} = G'_z \tag{2}$$

$$\bar{I}_x\ddot{\gamma} + \bar{c}_x\dot{\gamma} = G_x \tag{3}$$

where m represents beam mass per unit length; $\bar{I}_x$ is the moment of inertia along x-axis; ($\dot{}$) denotes $d/d\bar{t}$; ( )' represents $d/d\bar{x}$; $\bar{c}_y$ and $\bar{c}_z$ are the respective damping coefficients in the y and z directions; v, w, and γ denote the displacement (or twisting angle) in the y, z, and x directions. For a

homogeneous and isotropic beam, G_y, G_z, and G_x are defined as

$$G_y = -(D_{zz}v'')' - D_{xx}(\gamma' w'') - D_{zz}v'(v'v'' + w'w'')'$$
$$+ (D_{yy} - D_{zz})[(w''\gamma - v''\gamma^2)' - w'''\int_0^{\bar{x}} v''w'd\bar{x}]$$
$$- (1/2)v'\int_{\bar{l}}^{\bar{x}} m\frac{\partial^2}{\partial \bar{t}^2}(\int_0^{\bar{x}}(v'^2 + w'^2)d\bar{x})d\bar{x} + \bar{F}_y \quad (4)$$

$$G_z = -(D_{yy}w'')' + D_{xx}(\gamma' v'') - D_{yy}w'(v'v'' + w'w'')'$$
$$+ (D_{yy} - D_{zz})[(v''\gamma + w''\gamma^2)' + v'''\int_0^{\bar{x}} w''v'd\bar{x}]$$
$$- (1/2)w'\int_{\bar{l}}^{\bar{x}} m\frac{\partial^2}{\partial \bar{t}^2}(\int_0^{\bar{x}}(v'^2 + w'^2)d\bar{x})d\bar{x} + \bar{F}_z \quad (5)$$

$$G_x = (D_{xx}\gamma')' + (D_{zz} - D_{yy})[(v''^2 - w''^2)\gamma - v''w''] \quad (6)$$

where $D_{xx} = G\bar{I}_x$; $D_{yy} = E\bar{I}_y$; $D_{zz} = E\bar{I}_z$; G is the shear modulus, and E is Young's modulus. By substituting Eqs. (4~6) into Eqs. (1~3) and setting dimensionless coefficients $x = \bar{x}/\bar{l}$, $t = \bar{t}\omega$, $\omega = \sqrt{D_{yy}/m\bar{l}^4}$, $c_y = \bar{c}_y\bar{l}^2/\sqrt{mD_{yy}}$, $c_z = \bar{c}_z\bar{l}^2/\sqrt{mD_{yy}}$, $c_x = \bar{c}_x\bar{l}^2/\sqrt{mD_{yy}}$, $\mu_{xy} = D_{xx}/D_{yy}$, $\mu_{zy} = D_{zz}/D_{yy}$, where $\bar{l}$ is beam length, the flexural-flexural vibration equation of the 3D homogeneous and isotropic beam can be written as

$$\ddot{y} + c_y\dot{y} + \mu_{zy}y^{iv} = -\mu_{xy}(\gamma' w'')'$$
$$-(1-\mu_{zy})[(v''\gamma^2 - w''\gamma)' + z'''\int_0^x y''z'dx]'$$
$$-\mu_{zy}[y'(y'y'' + z'z'')']'$$
$$-\frac{1}{2}\{y'\int_1^x \frac{\partial^2}{\partial t^2}[\int_0^x (y'^2 + z'^2)dx]dx\}' + \bar{F}_y \quad (7)$$

$$\ddot{z} + c_z\dot{z} + z^{iv} = \mu_{xy}(\gamma' v'')'$$
$$+(1-\mu_{zy})[(v''\gamma + w''\gamma^2)' + y'''\int_0^x y'z''dx]' - [z'(y'y'' + z'z'')']'$$
$$-\frac{1}{2}\{z'\int_1^x \frac{\partial^2}{\partial t^2}[\int_0^x (y'^2 + z'^2)dx]dx\}' + \bar{F}_z \quad (8)$$

$$\ddot{\gamma} + c_x\dot{\gamma} - (\mu_{xy}/I_x)\gamma'' = (\mu_{zy} - 1)/I_x(y''^2\gamma - z''^2\gamma - y''z'') \quad (9)$$

where $(\dot{\ })$ represents d/dt, and $(\ )'$ denotes d/dx. To simplify the symbols, we used the same symbol to define the dimensionless displacements of the beam and the three axes. Thus, y and z denote the dimensionless displacement functions of windward ($y = v/\bar{l}$) and transverse ($z = w/\bar{l}$) directions of the beam, respectively. This does not affect the results of the theoretical model. In Eq. (9), we assumed that all time differential terms equaled 0 and that the boundary condition was $\gamma(0,t) = \gamma'(1,t) = 0$. Thus, the twist angle relationship is

$$\gamma = \frac{\mu_{zy} - 1}{\mu_{xy}}\int_0^x (\int_1^x y''z''dx)dx \quad (10)$$

Using Eq. (10) and Eqs. (7, 8), we can rewrite the equation of the 3D homogeneous and isotropic flexural-flexural beam to

$$\ddot{y} + c_y\dot{y} + \mu_{zy}y^{iv} = (1-\mu_{zy})\left[z''\int_1^x y''z''dx - z'''\int_0^x y''z'dx\right]' -$$
$$\frac{(1-\mu_{zy})^2}{\mu_{xy}}\left[z''\int_0^x\int_1^x y''z''dxdx\right]'' - \mu_{zy}\left[y'(y'y'' + z'z'')'\right]'$$
$$-\frac{1}{2}\left\{y'\int_1^x \frac{\partial^2}{\partial t^2}\left[\int_0^x (y'^2 + z'^2)dx\right]dx\right\}' + F_y \quad (11)$$

$$\ddot{z} + c_z\dot{z} + z^{iv} = -(1-\mu_{zy})\left[y''\int_1^x y''z''dx - y'''\int_0^x z''y'dx\right]'$$
$$-\frac{(1-\mu_{zy})^2}{\mu_{xy}}\left[y''\int_0^x\int_1^x y''z''dxdx\right]'' - \left[z'(y'y'' + z'z'')'\right]'$$
$$-\frac{1}{2}\left\{z'\int_1^x \frac{\partial^2}{\partial t^2}\left[\int_0^x (y'^2 + z'^2)dx\right]dx\right\}' + F_z \quad (12)$$

where F_y and F_z indicate the dimensionless distributed forces of the tower in the y and z directions. As for the windward forces and transverse induced aerodynamic forces of the tower, we referred to the unsteady aerodynamic force presented by van Horssen (1988):

$$\bar{F}_D = \frac{\rho_a\bar{U}_y^2\bar{d}}{2}\left(a_{D0U} + \frac{a_{D1U}}{\bar{U}_y}\frac{\partial\bar{y}(\bar{x},\bar{t})}{\partial\bar{t}} + \frac{a_{D2U}}{\bar{U}_y^2}\frac{\partial\bar{y}^2(\bar{x},\bar{t})}{\partial\bar{t}} + \frac{a_{D3U}}{\bar{U}_y^3}\frac{\partial\bar{y}^3(\bar{x},\bar{t})}{\partial\bar{t}} + ...\right) \quad (13)$$

Nondimensionalizing Eq. (13) gives

$$F_D = \hat{a}_{D0U} + \hat{a}_{D1U}\dot{y} + \hat{a}_{D2U}\dot{y}^2 + \hat{a}_{D3U}\dot{y}^3 \quad (14)$$

where $\hat{a}_{D0U} = \frac{\rho_a\bar{d}\bar{U}_y^2 a_{D0U}}{2m\omega^2}$, $\hat{a}_{D1U} = \frac{\rho_a\bar{d}\bar{U}_y a_{D1U}}{2m\omega^2}$, $\hat{a}_{D2U} = \frac{\rho_a\bar{d}a_{D2U}}{2m\omega^2}$, and $\hat{a}_{D3U} = \frac{\rho_a\bar{d}a_{D3U}}{2m\omega^2\bar{U}_y}$ are the aerodynamic coefficients of the y direction, and $\bar{U}_y$ denotes the wind speed in the y direction. Furthermore, the transverse induced aerodynamic force of the tower is

$$\bar{F}_A = \frac{\rho_a\bar{U}_y^2\bar{d}}{2}\left(a_{A0U} + \frac{a_{A1U}}{\bar{U}_y}\frac{\partial\bar{Z}(\bar{x},\bar{t})}{\partial\bar{t}} + \frac{a_{A2U}}{\bar{U}_y^2}\frac{\partial\bar{Z}^2(\bar{x},\bar{t})}{\partial\bar{t}} + \frac{a_{A3U}}{\bar{U}_y^3}\frac{\partial\bar{Z}_3(\bar{x},\bar{t})}{\partial\bar{t}} + ...\right) \quad (15)$$

Nondimensionalizing Eq. (15) gives

$$F_A = \hat{a}_{A0U} + \hat{a}_{A1U}\dot{z} + \hat{a}_{A2U}\dot{z}^2 + \hat{a}_{A3U}\dot{z}^3 \quad (16)$$

where $\hat{a}_{A0U} = \frac{\rho_a\bar{d}\bar{U}_y^2 a_{A0U}}{2m\omega^2}$, $\hat{a}_{A1U} = \frac{\rho_a\bar{d}\bar{U}_y a_{A1U}}{2m\omega^2}$, $\hat{a}_{A2U} = \frac{\rho_a\bar{d}a_{A2U}}{2m\omega^2}$, and $\hat{a}_{A3U} = \frac{\rho_a\bar{d}a_{A3U}}{2m\omega^2\bar{U}_y}$ are the aerodynamic coefficients of the z direction.

The external forces applied by the ocean currents on the tower are expressed using an unsteady uniform distributed force:

$$F_S = \tilde{F}_S e^{i\Omega_s t} = \tilde{F}_S e^{i\omega_m T_0 + \sigma T_1} \quad (17)$$

Thus, F_y and F_z can be expressed as $F_y = F_D + F_S$ and

$F_z = F_A$, respectively.

As shown in Fig. 1 (b), F_D and F_A are applied to the tower between $l/4$ and l, whereas F_S is the ocean current force applied to the tower between 0 and $l/4$; F_D represents the external force of the wind on the tower in the y direction (as the drag force). We further assumed that F_A is the transverse induced force (in the z-direction, as the aerodynamic force) and is produced by the wind in the y direction. If $\overline{U}_y$ is also in unsteady form, then $\hat{a}_{D0U} = \tilde{a}_{D0U} e^{2i\Omega t}$, $\hat{a}_{D1U} = \tilde{a}_{D1U} e^{i\Omega t}$, $\hat{a}_{A0U} = \tilde{a}_{A0U} e^{2i\Omega t}$, and $\hat{a}_{A1U} = \tilde{a}_{A1U} e^{i\Omega t}$.

Two DRs were added on the beam in an attempt to prevent I.R. and reduce vibrations in the y and z directions. The DRs can be regarded as external forces produced by two TMDs in the y and z directions of the beam. They can therefore be directly added into the equations of motion during the system integration process. We will discuss the influence of the DRs on the system in a later section. As for the equation of motion of the DRs, we can derive the following based on Newton's 2nd law:

$$\overline{m}_{0r}\ddot{\overline{y}}_{Dr}(t) - \begin{bmatrix} \bar{f}_s\left(\bar{y}(\bar{d}_r,\bar{t}) - \bar{y}_{Dr}(\bar{t})\right) + \\ \bar{g}_s\left[\dot{\bar{y}}(\bar{d}_r,\bar{t}) - \dot{\bar{y}}_{Dr}(\bar{t})\right] \end{bmatrix} = 0, r=1,2 \quad (18)$$

Replacing the $\overline{y}_{Dr}$ with $\overline{z}_{Dr}$ in Eq. (18) produces the equation of motion for the z direction, where $\overline{m}_{01,2}$ denotes the mass of the first and second DRs; $\overline{y}_{D1,2}$ (or $\overline{z}_{D1,2}$) represents the displacement of the first and second DRs; $\bar{d}_{1,2}$ indicates the location of the first and second DRs on the beam, and $\bar{f}_s$ and $\bar{g}_s$ are respectively the spring constant and damping coefficient of the DRs. Dividing Eq. (18) by $m\bar{l}$ and letting $y_{Dr} = \overline{y}_{Dr}/\bar{l}$, $m_{01,2} = \overline{m}_{01,2}/m\bar{l}$, $g_s = \bar{g}_s/m\bar{l}\omega$, and $f_s = \bar{f}_s/m\bar{l}\omega^2$ gives the dimensionless equation of motion for the DRs:

$$m_{01,2}\frac{d^2 y_{Dr}}{dt^2} - g_s(\dot{y} - \dot{y}_{Dr}) - f_s(y - y_{Dr}) = 0, r=1,2 \quad (19)$$

Using Newton's 2nd law, we added the y-dir. and z-dir. equations of motion of the beam and the influence of the DRs on the beam in the y and z directions. The integrated dimensionless equation of motion of the nonlinear beam can thus be written as

$$\begin{aligned} &\ddot{y} + c_y\dot{y} + \mu_{zy}y^{iv} - (1-\mu_{zy})\left[z''\int_1^x y''z''dx - z'''\int_0^x y''z'dx\right]' \\ &+ \frac{(1-\mu_{zy})^2}{\mu_{xy}}\left[z''\int_0^x\int_1^x y''z''dxdx\right]'' \\ &+ \mu_{zy}\left[y'(y'y'' + z'z'')'\right]' + \frac{1}{2}\left\{y'\int_1^x \frac{\partial^2}{\partial t^2}\left[\int_0^x (y'^2 + z'^2)dx\right]dx\right\}' \\ &+ \{f_s[y(d_1,t) - y_{D1}] + g_s[\dot{y}(d_1,t) - \dot{y}_{D1}]\}\delta(x-d_1) \\ &+ \{f_s[y(d_2,t) - y_{D2}] + g_s[\dot{y}(d_2,t) - \dot{y}_{D2}]\}\delta(x-d_2) = F_y \end{aligned} \quad (20)$$

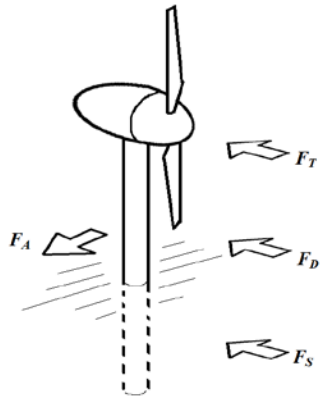

(a) Schematic model of wind-turbine tower

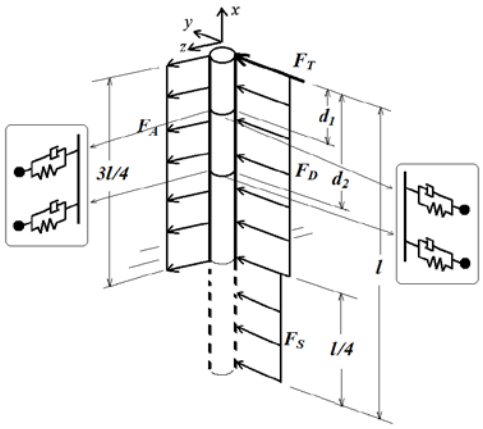

(b) Schematic model of multiple forces and DRs.

Fig.1 Schematic model of multiple forces applied to the wind-turbine tower

$$\begin{aligned} &\ddot{z} + c_z\dot{z} + z^{iv} + (1-\mu_{zy})\left[y''\int_1^x y''z''dx - y'''\int_0^x z''y'dx\right]' \\ &+ \frac{(1-\mu_{zy})^2}{\mu_{xy}}\left[y''\int_0^x\int_1^x y''z''dxdx\right]'' + \left[z'(z'z'' + y'y'')'\right]' \\ &+ \frac{1}{2}\left\{z'\int_1^x \frac{\partial^2}{\partial t^2}\left[\int_0^x (y'^2 + z'^2)dx\right]dx\right\}' + \{f_s[z(d_1,t) - z_{D1}] + \\ &g_s[\dot{z}(d_1,t) - \dot{z}_{D1r}]\}\delta(x-d_1) \\ &+ \{f_s[z(d_2,t) - z_{D2}] + g_s[\dot{z}(d_2,t) - \dot{z}_{D2}]\}\delta(x-d_2) = F_z \end{aligned} \quad (21)$$

where $\{f_s[y(d_r,t) - y_{Dr}] + g_s[\dot{y}(d_r,t) - \dot{y}_{Dr}]\}\delta(x-d_1)$, r =1,2, is the term for the DRs on the tower in the y direction, and $\{f_s[z(d_r,t) - z_{Dr}] + g_s[\dot{z}(d_r,t) - \dot{z}_{Dr}]\}$ $\delta(x-d_2)$, r =1,2, is the term for the DRs on the tower in the z direction. The dimensionless boundary conditions of the tower are

$$\begin{aligned} &y(0,t) = 0,\ y'(0,t) = 0,\ y''(l,t) = 0,\ y'''(l,t) = 0 \\ &z\ (0,t) = 0,\ z'(0,t) = 0,\ z''(l,t) = 0,\ z'''(l,t) = 0 \end{aligned} \quad (22)$$

Analysis by Using the Method of Multiple Scales (MOMS)

We adopted MOMS to analyze the frequency response and fixed points of the nonlinear equation, which involves dividing the time scale into fast and slow time scales. Suppose $T_0=\tau$ is the fast-time term, $T_1=\varepsilon^2\tau$ is the slow-time terms, and $y(x,t,\varepsilon)=\varepsilon y_0(x,T_0,T_1\cdots) \quad +\varepsilon^3 y_1(x,T_0,T_1\cdots)$, where ε is the time scale of small disturbances and is a minimum value. We disregard the influence of high-order terms such as $\varepsilon^5, \varepsilon^6$... on the system. Furthermore, we assumed that the cross-section of the beam is round, so the ratio of moment of inertia is 1. In other words, $\mu_{xy}=\mu_{zy}=1$; the structural damping is the same, so c_y = c_z = c. The method for the equation of motion in the *z* direction is identical to that for the *y* direction. We scale the dimensionless damping coefficient as $\varepsilon^2 c$. The damping and spring constant of the DRs are $\varepsilon^2 g_s$ and $\varepsilon^3 f_s$, respectively.

To facilitate our analysis, we only extracted the first two terms of the unsteady aerodynamic force for the external force applied to the tower and let the orders of $\hat{a}_{D0U}$ and $\hat{a}_{D1U}$ in the F_D equation be ε^3 and ε^2. Similarly, the orders of $\hat{a}_{A0U}$ and $\hat{a}_{A1U}$ in the F_A equation were set as ε^3 and ε^2. The order of the other uniform distributed force term F_S was set as ε^3. Thus, the order of ε^1 part in the equation of motion in the *y* direction is

$$\frac{\partial^2 y_0}{\partial T_0^2}+y_0^{iv}=0 \tag{24}$$

and ε^3 is

$$\begin{aligned}&\frac{\partial^2 y_1}{\partial T_0^2}+y_1^{iv}=-2\frac{\partial^2 y_0}{\partial T_0\partial T_1}-c_y\frac{\partial y_0}{\partial T_0}-\\&\frac{1}{2}\left\{y_0'\int_1^x\frac{\partial^2}{\partial t^2}\left[\int_0^x\left(y_0'^2+z_0'^2\right)dx\right]dx\right\}'\\&-\{y_0''^3+4y_0'y_0''y_0'''+y_0'^2y_0^{iv}+y_0''z_0''^2\\&+3y_0'z_0''z_0'''+y_0'z_0'z_0^{iv}+y_0''z_0'z_0'''\}\\&-\{f_s[y_1(d_1,t)-y_{D1}]+g_s[\dot{y}_1(d_1,t)-\dot{y}_{D1}]\}\delta(x-d_1)\\&-\{f_s[y_2(d_2,t)-y_{D2}]+g_s[\dot{y}_2(d_2,t)-\dot{y}_{D2}]\}\delta(x-d_2)\\&+\hat{a}_{D0U}+\varepsilon^3\hat{a}_{D1U}\frac{\partial y_0}{\partial T_0}+\tilde{F}_S e^{i\Omega_S t}\end{aligned} \tag{25}$$

Similarly, we can get the order of ε^1 and ε^3 part equations of motion in the *z* direction and would not detail here. Assuming that there is a wind turbine at the free end of the beam, then the dimensionless boundary conditions are as follows:

$$\begin{aligned}&y_0(0,t)=0,\ y_0'(0,t)=0,\ y_0''(l,t)=0,\ y_0'''(l,t)=\overline{F}_T e^{i\Omega_m t}\\&z_0(0,t)=0,\ z_0'(0,t)=0,\ z_0''(l,t)=0,\ z_0'''(l,t)=0\end{aligned} \tag{26}$$

This becomes a time-dependent boundary condition problem (Mindlin-Goodman (1950)) and will be discussed in the next section.

Analysis of Time Dependent Boundaries

We assume that y_0, the displacement of the tower can be written as

$$y_0(x,T_1,T_2)=v_0(x,t)+h_0(x)F_T(t) \tag{27}$$

where $v_0(x,t)$ is the transformed displacement; $h_0(x)$ denotes the shifting function, and $F_T(t)$ represents the forcing function. Substituting Eq. (27) into the boundary conditions of the beam produces the following:

$$\begin{aligned}&v_0(0,t)=-h_0(0)F_T(t),\ v_0'(0,t)=-h_0'(0)F_T(t),\\&v_0''(l,t)=-h_0''(l)F_T(t),\ v_0'''(l,t)=F_T(t)(1-h_0'''(l))\end{aligned} \tag{28}$$

For Eq. (28) to become homogeneous boundary conditions, the right side of the equations in Eq. (28) must equal 0. Accordingly, we can obtain the following boundary conditions of the shifting function:

$$h_0(0)=0,\ h_0'(0)=0,\ h_0''(l)=0,\ h_0'''(l)=1 \tag{29}$$

Assuming that $h_0(x)$ is a high-order polynomial,

$$h_0(x)=\alpha_0+\alpha_1 x+\alpha_2 x^2+\alpha_3 x^3 \tag{30}$$

After substituting Eq. (30) into Eq. (29), we can derive that $\alpha_0=\alpha_1=0,\quad \alpha_2=-l/2,\quad \alpha_3=1/6$, so the shifting function becomes $h_0(x)=-\frac{l}{2}x^2+\frac{1}{6}x^3$.

Furthermore, we assume that the generation solution to the transformed displacement (v_0) is $v_0(x,t)=\xi_{y0}\Phi(x)$, the boundary conditions of which are $v_0(0,t)=0$, $v_0'(0,t)=0$, $v_0''(l,t)=0$, $v_0'''(l,t)=0$. Also, let $\Phi(x)=E_1\cos\gamma x+E_2\sin\gamma x+E_3\cosh\gamma x+E_4\sinh\gamma x$. We can obtain the characteristic equation:

$$(-\sin^2\gamma l+\sinh^2\gamma l)-(\cos\gamma l+\cosh rl)^2=0 \tag{31}$$

Using the numerical method, we can obtain the first three eigenvalues of Eq. (31): 1.8751, 4.6941, and 7.7548. Then, based on the boundary conditions, we can derive the mode shape:

$$\begin{aligned}&\Phi_n(x)=(\cosh\gamma_n x-\cos\gamma_n x)-\\&\frac{\cos\gamma_n l+\cosh\gamma_n l}{\sin\gamma_n l+\sinh\gamma_n l}(\sinh\gamma_n x-\sin\gamma_n x)\end{aligned} \tag{32}$$

Finally, the solution to $y_0(x,t)$ can be written as

$$y_0(x,t)=\sum_{n=1}^{\infty}\xi_{y0n}\Phi_n(x)+h_0(x)F_T \tag{33}$$

where ξ_{y0n} is assumed to be

$$\xi_{y0n}=B_n(T_1)e^{-i\zeta_n}e^{i\omega_n T_0}+\overline{B}_n(T_1)e^{i\zeta_n}e^{-i\omega_n T_0}.$$

ANALYSIS OF INTERNAL RESONANCE CONDITIONS

System Without DRs

Before analyzing the influence of the DRs on tower vibrations, we must first discuss the nonlinear vibrations in the structure of the main body with no DRs and determine whether I.R. may take place. Thus, in this section, we removed the DR terms from Eqs. (20 and 21) and again adopted MOMS to derive ε^1 and ε^3 part equations of motion in the *y*, and z directions, respectively. Similarly, using the approach in Section 2, we let $y_1(x,t)=\sum_{n=1}^{\infty}\xi_{y1n}\Phi_n(x)$ and applied orthogonal properties. As the wind-turbine tower is symmetrical in the *y* and *z* directions, their mode frequencies are the same in all directions (*i.e.*, $\omega_{y1}=\omega_{z1}$, $\omega_{y2}=\omega_{z2}$ …). We verified that the eigen-values of the various modes in the same degree-of-freedom cannot form integer ratios in last Section. For this reason, the mode frequencies will not form integer ratios, either. In addition, the 1st mode is the fundamental mode of the tower, so we only consider the influence of the 1st mode here.

System Frequency Analysis

To examine the existence of I.R., we set the wind force function have a frequency of $\Omega=\omega_1+\varepsilon\sigma$, where ω_1 is the 1st mode's linear natural frequency and σ is the tuned frequency around the beam's linear natural frequency. As a result, when the external force excites the 1st mode in the *y* direction, secular terms with the exponent ω_1 must be selected. To determine the frequency responses of the system at fixed points (Fig. 2), we used numerical methods to obtain the amplitudes (B_y and B_z). We discovered that even if the tower is only subject to forces in the *y* direction, the amplitudes in the *z* direction are still significantly greater than those in the *y* direction. This is a typical I.R. phenomenon, which means that I.R. occurs in the tower. Next, we considered the induced force in the *z* direction. The resulting frequency responses are as shown in Fig. 3. We thus found a 19% increase in the amplitudes in the *z* direction, which was caused by the greater external force in said direction. Furthermore, as the tower is subject to forces in both the *y* and *z* directions, I.R. does not take place. This implies that if the wind force generates a transverse induced force, then I.R. will not take place in the tower. Nevertheless, the problem of vibration remains.

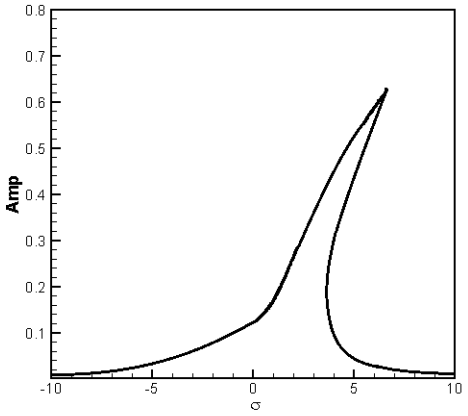

(a) 1st mode in *y*-dir.

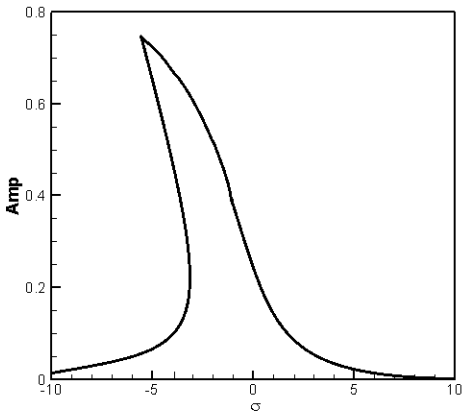

(b) 1st mode in *z*-dir.

Fig. 2 Fixed points plots of the amplitudes, force applied in the *y*-dir., no DRs.

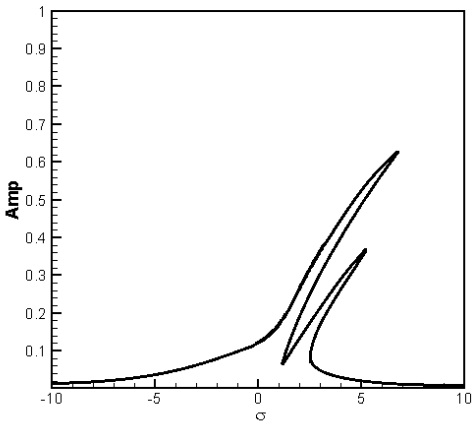

(a) 1st mode in *y*-dir.

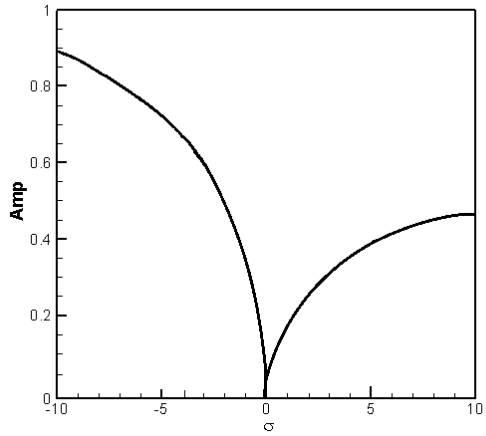

(b) 1st mode in *z*-dir.

Fig. 3 Fixed points plots of the amplitudes, forces applied in the *y*- and *z*-dirs., no DRs.

VIBRATION REDUCTION ANALYSIS OF SYSTEM WITH TMDs (DRs)

The results in last Section indicate that with no dampers and *y*-dir forces only, 1:1 I.R. occurs in the tower. We added the tower with two DRs in hopes of preventing I.R. and reducing to vibrations in the tower. The equations of motion of the two DRs are

$$m_{0r}\ddot{y}_{Dr} + g_s\dot{y}_{Dr} + f_s y_{Dr} = g_s\dot{y} + f_s y,$$
$$m_{0r}\ddot{z}_{Dr} + g_s\dot{z}_{Dr} + f_s z_{Dr} = g_s\dot{z} + f_s z,\ r=1,2 \quad (34)$$

where m_{01} and m_{02} respectively denote the mass ratios of the 1st and 2nd DRs; y_{D1} and y_{D2} (or z_{D1} and z_{D2}) indicate the displacement of the 1st and 2nd DRs; y and z represent the displacement of the tower in the y and z directions; f_s and g_s are the spring constant and damping coefficient of the DRs. We assumed that the displacement of the 1st DR (r=1) is $y_{D1} = A_{D1}e^{-i\zeta_y}e^{i\omega T_0}$ and $z_{D1} = B_{D1}e^{-i\zeta_z}e^{i\omega T_0}$, which, substituted into Eq. (34) give $A_{D1} = \dfrac{f_s B_y + f_s h_0(x)\bar{F}_T + i\omega B_y g_s + i\omega h_0(x)\bar{F}_T g_s}{-m_{01}\omega^2 + f_s + i\omega g_s}$ and $B_{D1} = \dfrac{f_s B_z + i\omega_1 B_z g_s}{-m_{01}\omega_1^2 + f_s + i\omega_1 g_s}$. Thus, the displacements of the DRs can be written as

$$y_{D1} = \frac{f_s B_y + f_s h_0(x)\bar{F}_T + i\omega B_y g_s + i\omega h_0(x)\bar{F}_T g_s}{-m_{01}\omega^2 + f_s + i\omega g_s} e^{-i\zeta_y}e^{i\omega T_0} \quad (35)$$

$$z_{D1} = \frac{f_s B_z + i\omega_1 B_z g_s}{-m_{01}\omega_1^2 + f_s + i\omega_1 g_s} e^{-i\zeta_z}e^{i\omega_1 T_0} \quad (36)$$

The analytical procedure for the 2nd DR (r=2) is the same, so we will not repeat it.

The method to obtain the *y*-dir and *z*-dir dynamic equations is identical to that used in the previous section for the tower with no DRs. After substituting Eqs. (35 and 36) into Eqs. (20 and 21), respectively, we applied orthogonal properties and multiplied both sides by Φ_j. Integrating from 0 to 1 then produces the *y*-dir and *z*-dir dynamic equations of the system with DRs.

We discuss the damping effects of the DRs on tower vibrations in two circumstances: when force is only applied in the *y* direction and when force is applied in the *y* and *z* directions, respectively. By drawing the frequency response plots (fixed points plots) for amplitudes B_y and B_z, the damping effects of the DRs can be observed. It is noted that the amplitude of the applied force on the tip ($F(t)$) does not have any effect on the system frequency. Therefore, the IR conditions will not be changed if we change the amplitude of the tip force. The amplitude of the tip force in the case we investigated was just an arbitrary chosen value. The effects of the DRs parameter combinations on the IR modes will not have much difference for a larger $F(t)$ amplitude. The results are discussed in the next section.

RESULTS AND DISCUSSION

In this section, we will discuss the damping effects of the DRs. We examined the location ($d_{1,2}$), mass ratio ($m_{01,02}$ and let m_{01}=m_{02}), spring constant (f_s), and damping coefficient (g_s) of the DRs to identify the optimal parameter combination. We considered two circumstances when the 1st mode in the *y* direction is excited: when force is only applied in the *y* direction and when force is applied in the *y* and *z* directions. According to Eqs. (24) & (26) and MOMS, the linear modes of the beam in the *y*- and *z*-dir. are decoupled. The tip force applies in the *y*-dir. will not affect the z-dir. vibrations of the beam. In other words, we can apply the tip force on the *y*-dir., the vibration and the DRs damping effects are the same as the case the tip force applied on the *z*-dir. In the present work, only *y*-dir. was investigated, the damping effects on the IR modes in the *z*-dir. are similar and not considered in this stage. We experimented on various parameter combinations **(***M* (mass ratio)=m_{01}+m_{02}= 0.001~0.01, d_1=0.35~0.75, d_2=0.1 (as shown in Fig. 1 (b)), f_s=0.1~1.0, g_s=0.1~1.0**)** and compiled the maximum amplitudes from their fixed points plots. Owing to the complexity of the data, only the results for g_s=1.0, f_s =0.1~1.0, M=0.001~0.01, d_1=0.35~0.75, and d_2=0.1 are listed in Tables 1 through 5. Tables 1 displays the maximum amplitudes in the system with no DRs when the 1st mode in the *y*-direction and *y*- and *z*-directions are excited. Table 2 presents the maximum amplitudes of the 1st mode in the system

with DRs when force is applied in only the y-direction with g_s=1.0 and f_s=0.1. Table 3 shows the maximum amplitudes in the system with DRs when force is applied in the y- and z-directions with f_s=0.1. Tables 4 and 5 are for the cases of DRs g_s=1.0 and f_s=1.0. The other combinations of f_s <1 are not shown in tables, because they do not give better damping effects than the case of f_s=1.0, g_s=1.0. Due to space limitations, we only present the other combinations in graphs.

Table 1. Max. Amplitudes of the 1st mode (No DRs)

	y	z
y-dir excited	0.626923084	0.745899022
y- and z-dir excited	0.613293886	0.8885595202

Table 2. Max. Amplitudes of the 1st mode when force is applied in the y-dir. (with DRs, f_s=0.1, g_s=1.0)

M (m_{01}=m_{02})	d_1 position	y	z
		Mode 1	Mode 1
0.001	0.35	0.379921913	0.00056942
0.004		0.37092191	0.000532631
0.007		0.369921923	0.000525594
0.01		0.365531206	0.000505772
0.001	0.45	0.370238215	0.000517836
0.004		0.368042886	0.000506824
0.007		0.364847571	0.000495962
0.01		0.36379683	0.000496002
0.001	0.55	0.372093707	0.000495581
0.004		0.366093606	0.00048686
0.007		0.364847601	0.000478319
0.01		0.367796809	0.000467969
0.001	0.65	0.360546827	0.000493559
0.004		0.361156106	0.000476748
0.007		0.360570192	0.000472615
0.01		0.360374898	0.000455791
0.001	0.75	0.357249886	0.000475417
0.004		0.35143739	0.000469515
0.007		0.34143737	0.000453933
0.01		0.335874915	0.000421571

Table 3. Max. Amplitudes of the 1st mode when forces are applied in the y- and z-dir. (with DRs, f_s=0.1, g_s=1.0)

M (m_{01}=m_{02})	d_1 position	y	z
		Mode 1	Mode 1
0.001	0.35	0.393807501	0.001597906
0.004		0.381636798	0.001386892
0.007		0.385346293	0.001389657
0.01		0.366251886	0.001387213
0.001	0.45	0.375650376	0.001435175
0.004		0.388129801	0.001268477
0.007		0.390076309	0.001280354
0.01		0.368356288	0.00125496
0.001	0.55	0.378174186	0.00137811
0.004		0.382523298	0.001348645
0.007		0.384702623	0.001319779
0.01		0.368662149	0.001260816
0.001	0.65	0.363228977	0.001383497
0.004		0.361853898	0.001239452
0.007		0.376315475	0.0012281
0.01		0.342574596	0.00108157
0.001	0.75	0.349812776	0.001296444
0.004		0.338683188	0.001221694
0.007		0.343617529	0.001234883
0.01		0.325585216	0.001059456

The results in Tables 1 through 3 reveal significantly smaller amplitudes in the y and z directions following the addition of the DRs. However, the vibration amplitudes in Tables 2 and 3 are for small values of g_s. Tables 4 and 5 present the best combinations of the DRs damping effect when the 1st mode in the y-direction and y- and z-directions are excited, respectively. The damping effects can be seen by comparing Tables 1 and 4 & 5. For example, the vibration amplitudes in the y-dir. were reduced from 0.626923084 (see Table 1, 1st row) to 0.325124413 (see Table 4, M=0.01, d_1=0.75) and 48.14% was reduced for the case of y-direction excited. And the vibration amplitudes in the y-dir. were reduced from 0.613293886 (see Table 1, 2nd row) to 0.265911639 (see Table 5, M=0.01, d_1=0.75) and 56.64% was reduced for the case of y- and z-direction excited. As can be seen, the amplitudes in the y and z directions are smaller than those produced in circumstances

with no DRs (such as Fig. 3). Also, the amplitudes in the *y* direction are again greater. These results demonstrate that adding the DRs can effectively prevent I.R.

Table 4. Max. Amplitudes of the 1st mode when forces are applied in the *y*- dir. (with DRs, f_s=1.0, g_s=1.0)

M (m_{01}=m_{02})	d_1 position	*y*	*z*
		Mode 1	Mode 1
0.001	0.35	0.360918194	0.00125036
0.004		0.350178242	0.001176624
0.007		0.354426414	0.001180026
0.01		0.32983315	0.001145385
0.001	0.45	0.358156204	0.000454637
0.004		0.3579804	0.000435685
0.007		0.357249886	0.000421628
0.01		0.352562398	0.000419895
0.001	0.55	0.355687499	0.000420353
0.004		0.352562398	0.000408576
0.007		0.349437386	0.000389419
0.01		0.35087499	0.000388857
0.001	0.65	0.344437391	0.000414367
0.004		0.34787491	0.000393239
0.007		0.347184509	0.000394132
0.01		0.344359309	0.000378591
0.001	0.75	0.342217296	0.000399739
0.004		0.339153379	0.000380107
0.007		0.328658193	0.000357777
0.01		0.325124413	0.000338447

In place of complex data tables for subsequent analysis, we drew the 3D plots for the various parameter combinations. Figure 4(a) and (b) are the 3D plots resulting from when force is only applied in the *y* direction with f_s = 0.1 ~ 1.0, and g_s = 0.1 and 1.0, respectively. Figure 5(a) and (b) are the 3D plots resulting from when force is applied in the *y* and *z* directions with f_s = 0.1 ~ 1.0, and g_s = 0.1 and 1.0, respectively. In these 3D plots, the *x* axis presents the mass ratio of the DRs; the *y* axis measures d_1, the distance between the 1st DR and the top of the tower (d_2 fixed at 0.1), and the *z* axis shows the corresponding maximum amplitudes in the *y* and *z* directions.

Table 5. Max. Amplitudes of the 1st mode when forces are applied in the *y*- and *z*-dir. (with DRs, f_s=1.0, g_s=1.0)

M (m_{01}=m_{02})	d_1 position	*y*	*z*
		Mode 1	Mode 1
0.001	0.35	0.360918194	0.00125036
0.004		0.350178242	0.001176624
0.007		0.354426414	0.001180026
0.01		0.32983315	0.001145385
0.001	0.45	0.345383406	0.001132809
0.004		0.353303701	0.001140665
0.007		0.358975411	0.001115947
0.01		0.328342259	0.0010778
0.001	0.55	0.341809273	0.001120912
0.004		0.345143884	0.001188768
0.007		0.373813212	0.001177575
0.01		0.327665627	0.001079769
0.001	0.65	0.320011586	0.001147044
0.004		0.331910402	0.001048723
0.007		0.336176008	0.001017162
0.01		0.285969913	0.000930821
0.001	0.75	0.305324793	0.001081435
0.004		0.287430674	0.000981702
0.007		0.289814591	0.0010222
0.01		0.265911639	0.000861141

In Figs. 4 and 5, different amplitude intervals are differentiated by color. For the mesh surface outlined in red, f_s =0.1, whereas f_s=0.4, 0.7 and 1.0 for the mesh surfaces outlined in blue, black and pink, respectively. The brown mesh surface presents the amplitudes in the tower not equipped with DRs. The graphs use different contour colors to differentiate the amplitudes; red indicates greater amplitudes and blue signifies smaller amplitudes associated with better damping effects. As the maximum amplitudes resulting the presence and absence of DRs differ considerably, it is difficult to make out the differences among different parameter combinations in circumstances with the DRs (such as in Fig. 4 (a)).

We therefore enlarged the lower portions of the 3D plots, as shown in Figs. 4 (b) and 5, and display the enlarged portions for the remainder of the figures. To facilitate result analysis, we selected the more representative figures for comparison. We first look at the vibrations in the tower in the *y* direction. When force is only applied in the *y* direction, Figs. 4 (a) and (b) show that a greater mass ratio and a greater distance between the two DRs result in smaller amplitudes in the *y* direction. Tower vibrations can be reduced regardless of f_s (maximum amplitudes smaller than when no DRs are used). When force is applied in the *y* and *z* directions, Figs. 5 (a) and (b) indicate that a greater mass ratio and a greater distance between the two DRs also result in smaller amplitudes in the *y* direction. Furthermore, tower vibrations can be reduced regardless of f_s. Following a comprehensive look at the entire tower, we discovered that the optimal damping effects in the *y* and *z* directions appeared when g_s=1.0, f_s=1.0, M=0.01, d_2=0.1, and d_1= 0.75, regardless of whether force is applied in only the *y* direction or in both the *y* and *z* directions (maximum amplitudes smaller than when no DRs are used). This shows that the DRs successfully prevent I.R. and can mitigate tower vibrations.

To further analysis of the damping effects of DRs' parameter combinations, we compiled a 3D maximum amplitude contour plot (3D MACP) for the DRs' parameters. Figure 6 is the 3D MACP for when force is applied in the *y* and *z* directions with g_s=1.0 and f_s=1.0. To verify the accuracy of 3D MACPs, we used numerical analysis to analyze Fig. 6, in which appeared the best damping effects. Orthogonalizing the Eqs. (20 and 21) produces the dynamic equations in the *y*- and *z*- direction, respectively. We employ the Runge-Kutta (RK4) numerical method and compiled the time response plot. Figure 6 is the circumstances in which force is only applied in the *y* and z direction, respectively. The graph in the upper left corner of the former is the time response plot for M=0.01, g_s=1.0, f_s=1.0, d_2=0.1, and d_1= 0.75. Again, the convergence value of the time responses is identical to the amplitude value of the designated point in the 3D MACP.

Based on Fig. 6, we found that the optimal locations are 0.75*l* from the top of the tower for the first DR and 0.1*l* from the top of the tower for the second DR. Also, their optimal parameters are g_s=1.0 and f_s=1.0. With the wind turbine situated at the top of the top, the maximum amplitude in the mode shape if the 1st mode of this free beam falls between 0.8*l* and *l*, which also means maximum displacement. Installing the TMD (or DR) where the displacement is greatest will have the best effects. This result is consistent with the inferences made by Wang and Tu (2016). We compared our results with the DRs actually applied to the Maokong Gondola towers in Taiwan, which are situated near the top and at 0.25*l* from the top of the towers to achieve damping where maximum displacement takes place (for details, please refer to Figure 7). The tower in this study is also subject to external force from the ocean current between 0 *l* and 1/4 *l*, which means that another TMD (or DR) is needed here. Thus, in addition to placing a DR near the top of the tower, we also suggest adding another set of DRs to the bottom fourth of the tower for even better damping effects.

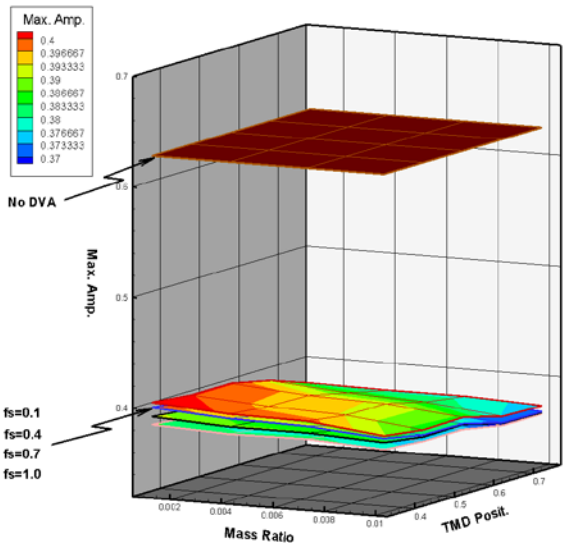

(a) g_s=0.1

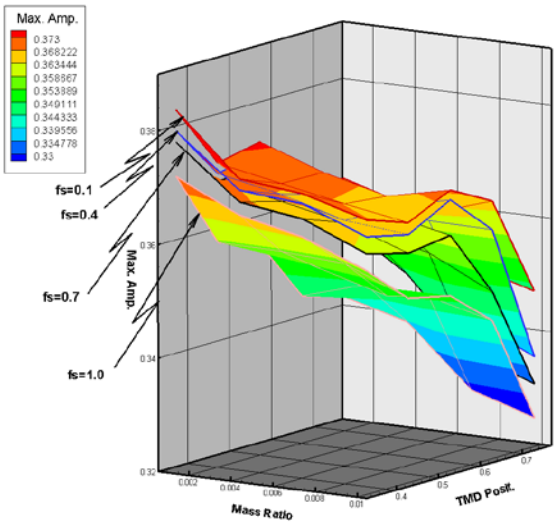

(b) g_s=1.0

Fig. 4 3D plots of the *y*-dir. 1st mode amplitudes, force applied in the *y*-dir., with DRs.

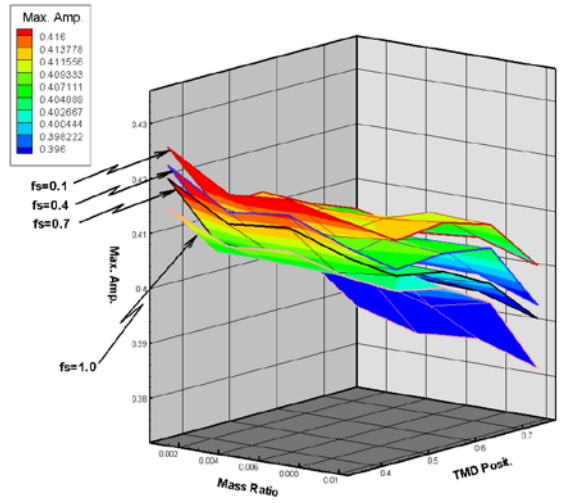

(a) g_s=0.1

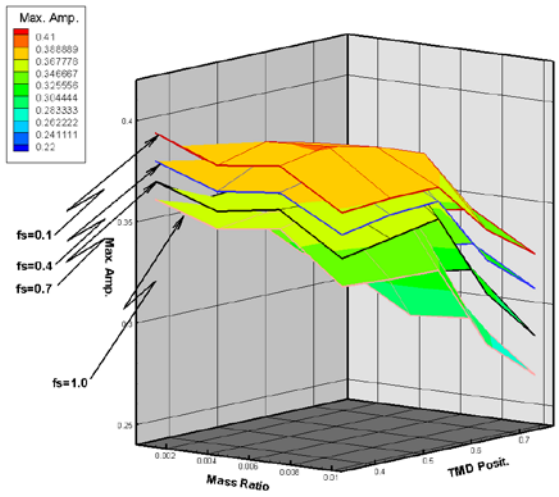

(b) g_s=1.0

Fig. 5 3D plots of the *y*-dir. 1st mode amplitudes, forces applied in the *y*- and *z*-dirs., with DRs.

CONCLUSIONS

The model established in this study is a 3D nonlinear wind-turbine tower with one fixed end and one free end. The symmetry of tower cross-section indicates the possibility of the 1:1 I.R. that is characteristic of nonlinear beams. We equipped the tower with two DRs and assumed that the bottom fourth of the tower is subject to the influence of ocean currents and that the rest of the beam is subject to the influence of wind. Furthermore, the wind turbine also applies force to the top of the tower. We examined the damping effects of the DRs and compared various combinations of mass, location, spring constant, and damping coefficient. The results were analyzed using MOMS, fixed point plots, and 3D MACPs, the accuracy of which was verified using the 4th order Runge-Kutta (RK4) method. Finally, we arrived at the following conclusions based on the results of this study:

1. As the wind-turbine tower is symmetrical in the *y* and *z* directions, their mode frequencies are the same in all directions (i.e., $\omega_{y1} = \omega_{z1}$, $\omega_{y2} = \omega_{z2}$ …), and this creates the possibility for I.R. in the *y* and *z* directions.
2. In addition to preventing I.R., the DRs can also reduce vibrations.
3. We found the optimal damping effects being up to 56.64% vibration reduction in the y-dir. with parameter combination g_s=1.0, f_s=1.0, and M=0.01, regardless of whether force is applied in only the *y* direction or in both the *y* and *z* directions.
4. The wind-turbine tower system is subject to multiple external forces, including ocean currents, aerodynamic force, and the wind turbine at the top of the tower. The results indicate that in addition to placing the DRs where the maximum amplitude appears in the beam mode shape, adding another set of DRs where the ocean currents and aerodynamic forces meet will produce better damping effects. For example, the maximum amplitude in the mode shape of the 1st mode of the fixed-free beam appears between 0.8*l* and *l*, so one of the DRs should be placed between 0.8*l* and *l*; the ocean current applies force to the bottom fourth of the tower, so placing another DR at 0.25*l* will provide the best damping effects.

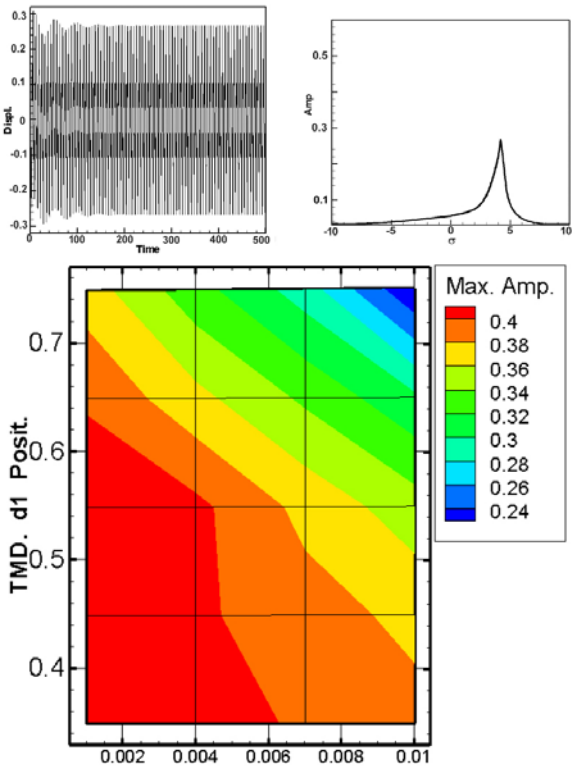

Fig. 6 3D MACPs of the 1st mode in *y*-dir., g_s=1.0, f_s=1.0.

Fig. 7 An example of the damping rings (the red rings near the top of the tower) applied to the Maokong Gondola towers in Taiwan.

REFERENCES

4C Offshore News, http://www.4coffshore.com/windfarms/windspeeds.aspx, (2017)

Brodersen, M. L. and Høgsberg, J., "Damping of offshore wind turbine tower vibrations by a stroke amplifying brace," *Energy Procedia*, Vol. 53, pp.258-267, (2014).

Colwell, S. and Basu, B., "Tuned liquid column dampers in offshore wind turbines for structural control," *Engineering Structures*, Vol. 31, pp.358-368, (2009).

Enevoldsen, I. and Mørk, K.J., "Effects of a vibration mass damper in a wind turbine tower," *Mechanics of Structures and Machines*, Vol. 24, No.2, pp.155-187, (1996).

Mindlin, R.D. and Goodman, L.E., "Beam Vibration with Time-Dependent Boundary Conditions," *ASME Journal of Applied Mechanics*, Vol. 17, pp. 377-380, (1950).

Nayfeh, A.H. and Pai, P.F., *Linear and nonlinear structural Mechanics*, John Wiley & Sons, Inc. Hoboken, New Jersey, (2004).

Oguamanam, D.C.D., "Free vibration of beams with finite mass rigid tip load and flexural- torsional coupling," *International Journal of Mechanical Sciences*, Vol.45, pp. 963–979, (2003).

Pai, P.F., *Nonlinear flexural-flexural-torsional dynamics of metallic and composite beams*, Ph.D. thesis, Virginia Polytechnic Institute and State University, (1990).

Stoykov, S. and Ribeiro, P., "Stability of nonlinear periodic vibrations of 3D beams," *Nonlinear Dynamics*, Vol. 66, pp. 335–353, (2011).

van Horssen, W. T., " An asymptotic theory for a class of initial-boundary value problems for weakly nonlinear wave equations with an application to a model of the galloping oscillations of overhead transmission lines," *SIAM Journal of Applied Mathematics*, Vol. 48,No. 6, pp. 1227-1243, (1988).

Wang ,Y. R., Feng, C.K. and Chen, S.Y., "Damping effects of linear and nonlinear tuned mass dampers on nonlinear hinged-hinged beam," *Journal of Sound and Vibration*, Vol. 430, pp. 150-173, (2018).

Wang, Y. R. and Lin, H. S., "Stability analysis and vibration reduction for a two -dimensional nonlinear system," *International Journal of Structural Stability and Dynamics*, Vol. 13, No. 5, article Number: 1350031, 33 pages, (2013).

Wang ,Y. R., and Lu, H. G., "Damping performance of dynamic vibration absorber in nonlinear simple beam with 1:3 internal resonance," *International Journal of Acoustics and Vibration*, Vol. 22, No.2, pp.167-185, (2017).

Wang, Y. R. and Wu, L. P., "Effects of Tuned Mass Damper on Fixed-Fixed 3D Nonlinear String Resting on Nonlinear Elastic Foundation," *International Journal of Structural Stability and Dynamics*, Vol. 17. No. 4, 33 pages, (2016).

Wang, Y. R. and Kuo, T. H., "Effects of a dynamic vibration absorber on nonlinear hinged-free beam," *Journal of Engineering Mechanics-ASCE*, Vol. 142, No. 4, 25 pages, (2016).

Wang, Y. R. and Liang, T. W., "Application of lumped-mass vibration absorber on the vibration reduction of a nonlinear beam-spring-mass system with internal resonances," *Journal of Sound and Vibration*, Vol. 350, pp. 140-170, (2015).

Wang, Y. R. and Tu, S. C., "Influence of tuned mass damper on fixed-free 3D nonlinear beam embedded in nonlinear elastic foundation," *Meccanica*, Vol. 51, No.10, pp. 2377-2416, (2016).

Zhang, Z., Nielsen, S. R. K., Blaabjerg, F. and Zhou, D., "Dynamics and control of lateral tower vibrations in offshore wind turbines by means of active generator torque," *Energies*, Vol. 7, pp. 7746-7772, (2014).

NOMENCLATURE

$\hat{a}_{A0,1,2,3U}$ =dimensionless aerodynamic coefficients in the *z* direction

$\hat{a}_{D0,1,2,3U}$ = dimensionless aerodynamic coefficients in the *y* direction

$\tilde{a}_{A,D0,1U}$ = magnitude of $\hat{a}_{A,D0,1U}$

c_y and c_z= dimensionless damping coefficients in the

y and z directions

$d_{1,2}$= dimensionless location of the first and second DRs on the beam

f_s and g_s= dimensionless spring constant and damping coefficient of the DRs

$m_{01,2}$= dimensionless mass of the first and second DRs

$y_{D1,2}$ (or $z_{D1,2}$) = dimensionless displacement of the 1st and 2nd DRs

Φ_n = mode shape of the n^{th} mode

Ω = wind force function frequency

ω_n = n^{th} mode's linear natural frequency

ξ_n = generalized coordinate of the n^{th} mode

ζ_n = phase angle of the n^{th} mode

減振環對於 3D 非線性細長樑受多重外力之減振效益的探討

王怡仁
淡江大學航太工程學系

蕭宛琪
雙鴻科技公司

摘要

本研究以一細長之非線性樑模擬近海風場風機塔柱受多重外力時，產生振動之現象。吾人考慮的外力為：迎風向的空氣阻力，側向的空氣力，以及迎風向彈性樑自由端 (tip free end) 的風機所施予之點受力；另外還考慮海面下的洋流外力。吾人將利用 Mindlin-Goodman 及時間多尺度法 (method of multiple scales (MOMS)) 分析此時變性邊界條件及非線性的氣體彈性問題，並使用兩減振環裝設於風機塔柱上，達到避開內共振，並有最佳之減振效果。